## 3.2 PROPERTIES OF DEFECTS AND IMPLANTS IN $Mg^+$ IMPLANTED SILICON CARBIDE

— W. Jiang, Z. Zhu, T. Varga, M. E. Bowden, S. Manandhar, T. Roosendaal, S. Y. Hu, C. H. Henager, Jr., R. J. Kurtz, (Pacific Northwest National Laboratory); and Y. Wang (Los Alamos National Laboratory)

### OBJECTIVE

As a candidate material for fusion reactor designs, silicon carbide (SiC) under high-energy neutron irradiation undergoes atomic displacement damage and transmutation reactions that create magnesium as one of the major metallic products. The presence of Mg and lattice disorder in SiC is expected to affect structural stability and degrade thermo-mechanical properties that could limit SiC lifetime for service. We have initiated a combined experimental and computational study that uses $Mg^+$ ion implantation and multiscale modeling to investigate the structural and chemical effects in Mg implanted SiC and explore possible property degradation mechanisms.

### SUMMARY

Implantation of 3C-SiC, 6H-SiC and CVD-SiC has been performed with 200 keV $Mg^+$ ions to fluences up to $3.2\times10^{16}$ ions/cm$^2$ at 773 K. Rutherford backscattering analyses of the as-produced damage states along multiaxial channeling directions indicate that there are interstitial-type defect configurations that are well aligned with the <100> axis, such as Si-Si <100> interstitial splits. The depth profile of the as-implanted Mg exhibits a Gaussian-like distribution without evidence of considerable diffusion-driven mass transport during implantation. A post implantation thermal annealing study shows that there is a significant recovery of the structural defects with essentially immobile Mg in SiC up to 1473 K. Further annealing at higher temperatures is currently in progress with intent to recover implantation damage to the maximum extent possible while retaining Mg implants in the sample. Characterizations will follow using spectroscopy and microscopy to study microstructure and Mg behavior in SiC.

### PROGRESS AND STATUS

#### Introduction

Due to their outstanding properties and attractive features, silicon carbide composites (SiC/SiC) have been investigated as candidates for structural materials [1] and flow channel inserts [2] in the designs of fusion power plants. The materials will be subjected to high-energy neutron irradiation in the fusion environment, resulting in elemental transmutations and atomic displacements. Recent calculations by Sawan, *et al*. [3] predict that at a fast neutron dose of ~100 dpa (displacements per atom), there will be ~0.5 at.% Mg generated in SiC among other major transmutants that include 0.15 at.% Al, 0.2 at.% Be, 0.01 at.% P, 2.2 at.% He and 0.84 at.% H through (n,$\alpha$), (n,d) and (n,$\beta^-\gamma$) nuclear reactions. The effects of those impurities in SiC on structural stability and thermo-mechanical properties are currently unknown and need to be studied in order to assess property degradation that could limit the material lifetime for service. We have initiated a study that uses a combination of $Mg^+$ ion-implantation and multiscale modeling to simulate and examine the structural and chemical effects. The goal is to identify and understand the Mg roles in disordered SiC structure and to assess its impact on properties. This initial experimental report summarizes the data on the defect accumulation and recovery as well as Mg behavior in implanted and annealed SiC. Further studies will address

microstructures, Mg locations, possible Mg-containing precipitates, swelling in conjunction with helium, grain boundaries, etc.

**Experimental Procedure**

Three polymorphs of 3C-SiC single-crystal film on Si substrate, 6H-SiC single-crystal wafer, and polycrystalline CVD-SiC bulk were implanted 7° off normal with 200 keV $Mg^+$ ions to fluences up to $3.2\times10^{16}$ ions/cm$^2$ at 773 K. The elevated temperature was applied to avoid full amorphization in SiC. The maximum ion fluence corresponds to a dose of ~18 dpa at the damage peak according to SRIM simulation [4], where the threshold displacement energies for C and Si in SiC are assumed to be 20 and 35 eV, respectively. The epitaxial film used in this study was determined by pole-figure measurements (data not shown) to be single-crystal 3C-SiC with (100) orientation. Exfoliation in some areas of the 3C-SiC film (~2 μm thick) occurred during ion implantation. 3C-SiC single crystal is chosen in this study because it has the same crystal structure of potentially used SiC/SiC and should allow for a detailed study of damage states and Mg locations in the crystal structure. CVD-SiC is used to study any grain-boundary effects on Mg transport. X-ray diffraction (XRD) analysis (data not shown) shows that the CVD-SiC in this study is a single phase of 3C-SiC with an average grain size of ~33 nm. The 6H-SiC single-crystal wafer obtained from Cree has high crystalline quality and serves as a 3C-SiC surrogate for studying damage accumulation and recovery as well as Mg behavior.

Multiaxial ion channeling [5] based on 2.0 MeV $He^+$ Rutherford backscattering spectrometry (RBS/C) was used to analyze the lattice disorder on the Si sublattice in the $Mg^+$ ion implanted 3C-SiC. Time-of-flight secondary ion mass spectrometry (ToF-SIMS) was applied to profile Mg implants in both 6H-SiC and CVD-SiC. Isochronal (2 hours) annealing at temperatures up to 1473 K in an Ar environment was conducted and the same characterization methods were employed to study damage recovery and thermal behavior of Mg in the SiC samples. Further annealing at higher temperatures is currently in progress. These step-by-step procedures are needed to recover implantation-induced defects to the maximum extent possible while retaining a majority of Mg in SiC. The annealed samples will be characterized using a variety of methods, including PIXE (Particle-Induced X-ray Emission) or PIGE (Particle-Induced γ-ray Emission) under multiaxial channeling conditions, TEM (transmission electron microscopy) and APT (atom probe tomography) to identify Mg locations in the crystal structure, microstructural features, defect configurations, minor phases, precipitates, interfaces, etc.

**Results and Discussion**

RBS/C spectra along the <100>, <110> and <111> axes in 3C-SiC irradiated to $3.2\times10^{16}$ $Mg^+$/cm$^2$ at 773 K are shown in Figure 1. Also included are random and channeling spectra from an unirradiated area, which respectively define the upper and lower levels of the backscattering yields from the completely amorphized SiC material and essentially defect-free SiC crystal. According to Figure 1, the minimum yields for the Si sublattice in the unirradiated 3C-SiC are 2.8%, 3.6%, and 4.2%, as observed along the <110>, <100>, and <111> axes, respectively. The results indicate that the unirradiated 3C-SiC in the near-surface region of interest has high crystalline quality, as previously reported [6]. The depth scale for Si, shown on the top axis of Figure 1, is converted based on the SRIM-2003 database [4] of random stopping powers for both incoming and outgoing paths. The conversion also adopted a surface energy approximation [7]. The broad damage peak for the same damage states in the irradiated sample is apparent from observation along each axis. Because the RBS method used in this study does not resolve Mg and Si, the damage peak also includes Mg contributions. However, this contribution is negligibly small as compared to the percentage of Si displacements, about

2% vs. 50% or more (see Figure 2). The irradiated SiC is not fully amorphized because the sample temperature during irradiation was above the critical temperature for amorphization. At the elevated temperature (773 K), the interaction of point defects not only leads to simultaneous recovery to avoid full amorphization, but also formation of extended defects. The residual damage state in the as-implanted SiC is expected to contain a high concentration of defect clusters.

The relative disorder on the Si sublattice is obtained from the RBS/C spectra in Figure 1 using an iterative procedure [8,9] that is based on dechanneling from the actual disorder present. This procedure extracts the probability of close encounters between the energetic particles and the displaced atoms, which is directly proportional to the disorder concentration. The depth profiles of the relative disorder on the Si sublattice in the irradiated 3C-SiC observed along the <100>, <110>, and <111> axes are shown in Figure 2. The peak-fitted curves in the figure are to aid the eye. In the near-surface region, lattice disorder cannot be determined due to the influence of the surface peak from the surface-atom scattering. From Figure 2, the disorder levels on the Si sublattice observed along <110> and <111> are comparable in the depth region, but they are noticeably higher than along <100>. The data suggest that in addition to randomly distributed Si atoms around the damage peak, there are interstitial defect configurations that are well aligned with the <100> axis, such as Si-Si <100> interstitial splits. Those aligned Si atoms are effectively shielded by the <100> atomic rows, leading to a reduction in the dechanneling yield. Orientation dependence of Si disorder in 3C-SiC [6] and 6H-SiC [5] irradiated at low and room temperatures was also previously observed. Our recent *ab initio* calculation [10] on Mg-incorporated 3C-SiC reveals that although Si-Mg <100> and C-Mg <100> configurations are unstable, the energetically favored interstitial site of Mg is at the tetrahedral center of C. The Mg and Si interstitials align with the <100> axis. In addition, Si-Si <100> interstitial splits or dumbbells are stable with a relatively high defect formation energy (9.48 eV).

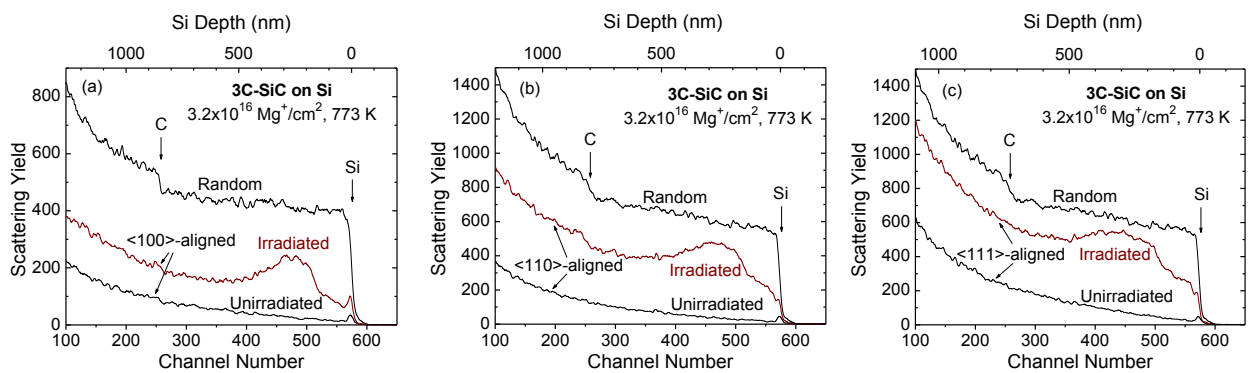


Figure 1. 2.0 MeV $He^+$ RBS/C spectra along (a) <100>, (b) <110> and (c) <111> axes for 3C-SiC irradiated with 200 keV $Mg^+$ to $3.2\times10^{16}$ ions/cm$^2$ at 773 K. Also included are random and channeling spectra from an unirradiated area.

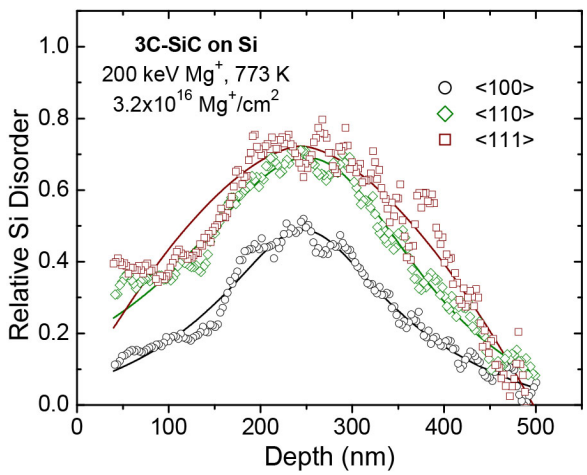


Figure 2. Depth profiles of disorder on the Si sublattice in 3C-SiC irradiated with 200 keV $Mg^+$ to $3.2\times10^{16}$ ions/cm$^2$ at 773 K, as observed along the <100>, <110> and <111> axes. Symbols are experimental data derived from Figure 1 and lines are drawn to aid the eye.

Figure 3 shows representative RBS/C spectra for 6H-SiC implanted to $2.5\times10^{16}$ $Mg^+$/cm$^2$ at 773 K and 2-hour isochronally annealed at 1073 and 1473 K. Channeling and random spectra from an unirradiated area are also included in the figure. It is apparent that as temperature increases, the intensity of the damage peak decreases, indicating that defect recovery occurs in the thermal annealing process. In general, the recovery behavior of 6H-SiC is similar to that of 3C-SiC [6] as the local tetrahedral structure in all SiC polymorphs is identical. Further annealing at higher temperatures, which is being conducted, may lead to more recovery of defects in the sample. It should be noted that at larger depths (>500 nm), the RBS/C spectrum for 1473 K is slightly higher than for 1073 K, primarily due to the additional damage produced by the 2.0 MeV $He^+$ ion beam that was used to refine the channeling direction and take the spectrum data in the same area.

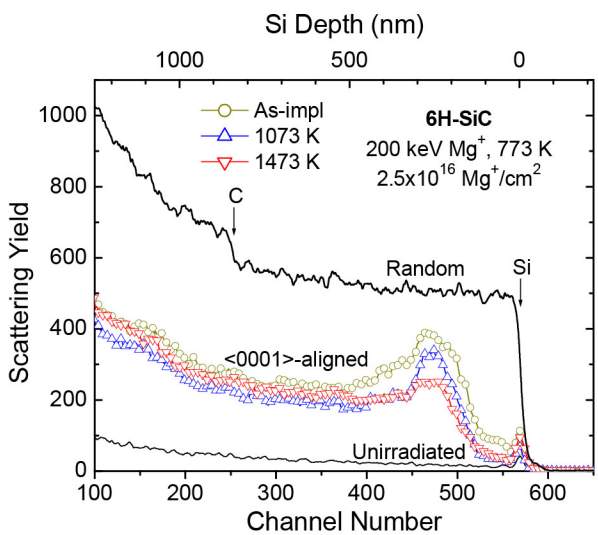


Figure 3. Isochronal (2 hours in Ar) annealing at 1073 and 1473 K for 6H-SiC irradiated with 200 keV $Mg^+$ to $2.5\times10^{16}$ ions/cm$^2$ at 773 K.

The implanted Mg in 6H-SiC and CVD-SiC following implantation at 773 K and thermal annealing up to 1473 K was analyzed using TOF-SIMS. The peak-height normalized profiles of the implanted Mg are shown in Figure 4 as a function of depth with ~1.6 at.% and ~2.0 at.% Mg at the peak maxima in 6H-SiC and CVD-SiC, respectively. The corresponding peak positions and widths are given in Table 1. The depth calibration for 6H-SiC was performed by measuring the depth of the sputtered craters. The accuracy for the depth measurement is within a few percent. Since the surface of the CVD-SiC sample is not very smooth microscopically, its depth scale is determined based on the sputtering rate in units of nm/(nA·sec) for 6H-SiC under the same sputtering conditions (2 keV $O^+$). The Mg profile in the as-implanted 6H-SiC in Figure 4(a) is located at 250 nm with FWHM = 103 nm. Annealing at higher temperatures up to 1473 K does not lead to a significant change in the peak shape and position, as shown in Figure 4(a). The peak width is also identical within the experimental error (Table 1). The data suggest that the implanted Mg in 6H-SiC structure is essentially immobile up to the high temperature (1473 K). This behavior is similar to Ag in crystalline and amorphized SiC at

elevated temperatures [11]. A similar conclusion for Mg in CVD-SiC can be drawn, which indicates that the grain boundaries in the polycrystalline CVD-SiC do not provide a faster diffusion path for Mg to migrate at temperatures up to 1473 K. It is noticed that the Mg peak position in CVD-SiC [Figure 4(b)] is comparable to that in 6H-SiC [Figure 4(a)], but its peak width is systematically larger by 20-30%, which could be attributed to the surface roughness. Further investigations are needed to determine how the implanted Mg is structurally and chemically incorporated in SiC and whether any Mg-containing precipitates are formed.

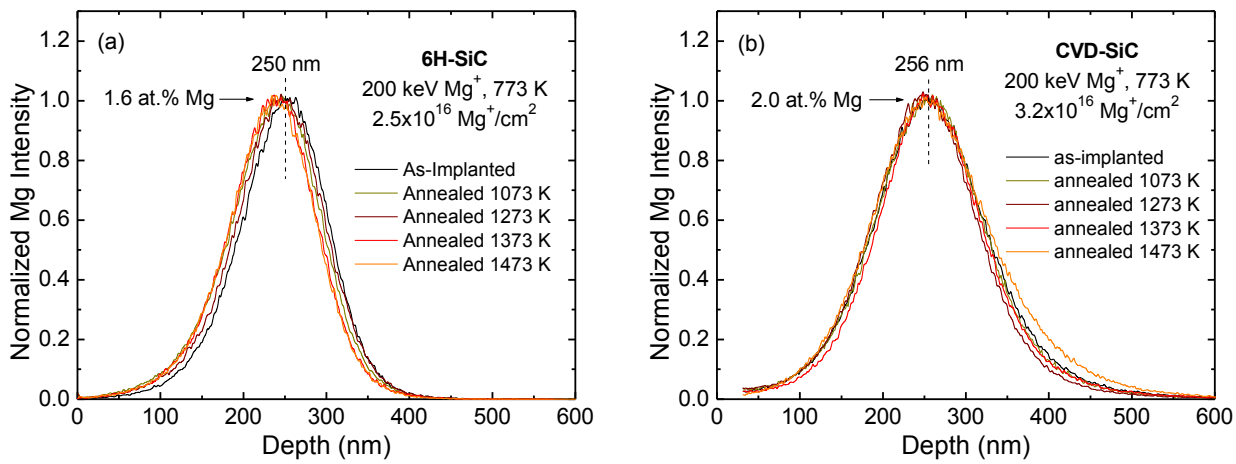


Figure 4. SIMS depth profiles of Mg in (a) 6H-SiC and (b) CVD-SiC implanted at 773 K and annealed at temperatures from 1073 to 1473 K for 2 hours at each temperature in an Ar environment.

Table 1. Peak position and width of implanted Mg in 6H-SiC and CVD-SiC.

| Implantation/Annealing Temperature (K) | Peak Position (nm) | | Peak FWHM (nm) | |
|---|---|---|---|---|
| | 6H-SiC | CVD-SiC | 6H-SiC | CVD-SiC |
| 773 | 250 | 256 | 103 | 135 |
| 1073 | 240 | 256 | 108 | 131 |
| 1273 | 245 | 250 | 106 | 127 |
| 1373 | 236 | 257 | 104 | 126 |
| 1473 | 235 | 258 | 104 | 147 |

Note: 1 Implantation was performed using 200 keV $Mg^+$ ions at 773 K. 2. Thermal annealing was conducted for 2 hours at each temperature in an Ar environment.

## ACKNOWLEDGEMENTS

This research was supported by Office of Fusion Energy Sciences, U.S. Department of Energy (DOE) under Contract DE-AC05-76RL01830. A portion of the research was performed using EMSL, a national scientific user facility sponsored by the DOE's Office of Biological and Environmental Research and located at PNNL. Ion implantation was conducted at Ion Beam

Materials Laboratory through a partial support from Center for Integrated Nanotechnologies in Los Alamos National Laboratory.

**REFERENCES**

[1] A. R. Raffray, R. Jones, G Aiello, M. Billone, L. Giancarli, H. Golfier, A. Hasegawa, Y. Katoh, A. Kohyama, S. Nishio, B. Riccardi, and M. S. Tillack, *Fusion Eng. Des.* **55** (2001) 55.
[2] C. P. C. Wong, M. Abdou, M. Dagher, Y. Katoh, R. J. Kurtz, S. Malang, E. P. Marriott, B. J. Merrill, K. Messadek, N. B. Morley, M. E. Sawan, S. Sharafat, S. Smolentsev, D. K. Sze, S. Willms, A. Ying, and M. Z. Youssef, *Fusion Eng. Des.* **85** (2010) 1129.
[3] M. E. Sawan, Y. Katoh, and L. L. Snead, *J. Nucl. Mater.*, in press (2013).
[4] J. F. Ziegler, J. P. Biearsack, and U. Littmark, "The stopping and Range of Ions in Solids," (Pergamon Press, New York, 1985); available from: http://www.SRIM.org/.
[5] W. Jiang and W. J. Weber, *Phys. Rev B* **64** (2001) 125206.
[6] W. Jiang, W. J. Weber, J. Lian, and N. M. Kalkhoran, *J. Appl. Phys. 105* (2009) 013529.
[7] W. K. Chu, J. W. Mayer, and M. A. Nicolet, "Backscattering Spectrometry," (Academic Press, San Diego, CA, 1978) 63.
[8] J. R. Tesmer and M. Nastasi, "Handbook of Modern Ion Beam Materials Analysis," (Materials Research Society, Pittsburgh, 1995) 267.
[9] J. R. Bird and J. S. Williams, "Ion Beams for Materials Analysis," (Academic Press, San Diego, 1989) 286.
[10] S. Y. Hu, W. Setyawan, R. van Ginhoven, W. Jiang, C. H. Henager, Jr. and R. J. Kurtz, *J. Nucl. Mater.,* submitted (2013).
[11] W. Jiang, W. J. Weber, V. Shutthanandan, L. Li, and S. Thevuthasan, *Nucl. Instr. Math. Phys. Res. B* **219-220** (2004) 642.